

Representing moisture fluxes and phase changes in glacier debris cover using a reservoir approach

E. Collier^{1,4}, L. I. Nicholson², B. W. Brock³, F. Maussion⁴, R. Essery⁵, and A. B. G. Bush¹

¹Department of Earth & Atmospheric Sciences, University of Alberta, Edmonton, Canada

²Institute of Meteorology and Geophysics, University of Innsbruck, Innsbruck, Austria

³Geography Department, Northumbria University, Newcastle upon Tyne, UK

⁴Chair of Climatology, Technische Universität Berlin, Berlin, Germany

⁵School of Geosciences, University of Edinburgh, Edinburgh, Scotland

Correspondence to: E. Collier (eec@ualberta.ca)

Abstract. Due to the complexity of treating moisture in supraglacial debris, surface energy balance models to date have neglected moisture infiltration and phase changes in the debris layer. The latent heat flux (QL) is also often excluded due to the uncertainty in determining the surface vapour pressure. To quantify the importance of moisture on the surface energy and climatic mass balance (CMB) of debris-covered glaciers, we developed a simple reservoir parameterization for the debris ice and water content, as well as an estimation of the latent heat flux. The parameterization was incorporated into a CMB model adapted for debris-covered glaciers. We present the results of two point simulations, using both our new “moist” and the conventional “dry” approaches, on the Miage Glacier, Italy, during summer 2008 and fall 2011. The former year coincides with available in-situ glaciological and meteorological measurements, including the first eddy-covariance measurements of the turbulent fluxes over supraglacial debris, while the latter contains two refreeze events that permit evaluation of the influence of phase changes. The simulations demonstrate a clear influence of moisture on the glacier energy and mass-balance dynamics. When water and ice are considered, heat transmission to the underlying glacier ice is lower, as the effective thermal diffusivity of the saturated debris layers are reduced by increases in both the density and specific heat capacity. In combination with surface heat extraction by QL, sub-debris ice melt is reduced by 3.1 % in 2008 and by 7.0 % in 2011 when moisture effects are included. However, the influence of the parameterization on the total accumulated mass balance varies seasonally. In summer 2008, mass loss due to surface vapour fluxes more than compensated the reduction in ice melt, such that the total ablation increased by 4.0 %.

Conversely, in fall 2011, the modulation of basal debris temperature by debris ice resulted in a decrease in total ablation, of 2.1 %. Although the parameterization is a simplified representation of the moist physics of glacier debris, it is a novel attempt at including moisture in a numerical model of debris-covered glaciers and opens up additional avenues of future research.

1 Introduction

Numerical modelling of debris-covered glaciers has received renewed scientific interest in recent years, as their contribution to changes in ice mass and water resources in many regions remains poorly understood (e.g. Käb et al., 2012) and due to the fact that the proportion of debris-covered glacier area is rising as glaciers recede (e.g. Stokes et al., 2007; Bolch et al., 2008; Bhambri et al., 2011).

It is well established that supraglacial debris exerts an important control on glacier melt rates. Sub-debris ice-melt is strongly enhanced when the debris thickness is less than a few centimeters, due to a reduction in surface albedo, an increase in absorption of shortwave radiation, and the rapid transfer of energy to the underlying ice. Melt decreases exponentially as the thickness increases, as a result of insulation of the underlying glacier ice from the overlying atmosphere (e.g. Østrem, 1959; Loomis, 1970; Fujii, 1977; Inoue and Yoshida, 1980; Mattson et al., 1993). The presence of debris also alters the glacier surface energy balance, by permitting surface temperatures to rise above the melting point and by altering surface heat and moisture exchanges with the atmosphere (e.g. Brock et al., 2010).

Numerous point models of the surface energy balance of debris-covered glaciers have been developed to simulate sub-debris ice melt (e.g. Kraus, 1975; Nakawo and Young, 1982; Han et al., 2006; Nicholson and Benn, 2006; Reid and Brock, 2010). In recent years, models of debris cover have been extended to distributed simulations (Zhang et al., 2011), and to include both explicit calculation of heat conduction through debris layers resolved into multiple levels and snow accumulation on top of the debris (Reid et al., 2012; Lejeune et al., 2013; Fyffe et al., 2014).

However, due to the complexity of treating moisture in supraglacial debris cover, surface energy balance models to date have neglected the latent heat and surface moisture flux components, with the exception of (1) testing the two end-member cases of completely dry or completely saturated debris layers (e.g. Nakawo and Young, 1981; Kayastha et al., 2000; Nicholson and Benn, 2006), and (2) using measurements of surface relative humidity to calculate the flux when the surface is saturated (Reid and Brock, 2010; Reid et al., 2012). In addition, moisture inputs to the debris layer – by percolation of snowmelt and rainfall, or from the underlying melting ice via capillary action – and their phase changes have not been taken into account. Rather, any water is assumed to run off immediately, without influencing the thermal properties of the debris (e.g. Reid and Brock, 2010; Reid et al., 2012; Lejeune et al., 2013; Fyffe et al., 2014).

Both field observations and laboratory experiments indicate that debris covers can be partially or entirely saturated at times during the ablation season, depending on the thickness and environmental conditions, with a minimum of a saturated region adjacent to the interface if the underlying ice is at the melting point (e.g. Nakawo and Young, 1981; Conway and Rasmussen, 2000; Kayastha et al., 2000; Reznichenko et al., 2010; Nicholson and Benn, 2012). The presence of interstitial water and ice modifies the thermal properties of the debris layer, particularly during transition seasons (e.g. Conway and Rasmussen, 2000; Nicholson and Benn, 2012). In addition, percolation of rain through a debris layer, which can reach as high as 75 % of the total rainfall at the surface (Sakai et al., 2004), and other inputs of moisture can influence the thermal regime by heat advection (Reznichenko et al., 2010), and by providing a source of moisture for evaporation that cools the debris and therefore reduces heat transmission to the ice below.

Surface vapour exchanges between the debris and the overlying atmosphere influence the surface energy balance and have been observed to be non-negligible at times. Sakai et al. (2004) estimated that the ablation calculated by an energy balance approach that neglects the latent heat flux, QL , would provide an overestimate by 100 %, since its lowering effect on surface temperature would not be captured. During the ablation season on the Miage glacier in the Italian Alps, Brock et al. (2010) calculated large spikes in QL , of up to -800 W m^{-2} , that coincided with daytime rainfall events on the heated debris surface. Furthermore, while they esti-

ated that energy inputs due to condensation and deposition were negligible, ground frosts were observed on a weekly to bi-weekly basis in the upper parts of the glacier, which may slow early daytime heating of the debris layer. Given the clear influence of moisture on the surface energy balance and the subsurface thermal regime, there is a need to develop a treatment for moisture fluxes into and within the debris layer, as well as for phase changes that would allow for a variation in the thermal properties and energy sources and sinks of the debris layer with depth and time.

In this paper, we explore the utility of a reservoir scheme for parameterizing moisture fluxes and phase changes in a glacier debris layer that has been incorporated into a glacier climatic mass balance model. We exploit a short period of available in-situ measurements over supraglacial debris to evaluate the model performance during an ablation season, with a second simulation of a fall season to fully demonstrate the capabilities of the model. Within the context of the simplified parameterization, we show the influence of moisture on heat transfer in the debris layer, its physical properties, and sub-debris ice melt, as well as assess the scale of the impact of phase changes. The eventual goal of this work is to incorporate the debris modifications into an interactively coupled modelling system of the atmosphere and alpine glaciers at the regional scale (Collier et al., 2013). The inclusion of debris is essential for (1) accurately capturing surface conditions over debris-covered glaciers and, therefore, atmosphere-glacier feedbacks, and (2) rigorously assessing regional climatic influences on the CMB of debris-covered glaciers.

2 Methods

2.1 Debris-free glacier CMB model

The debris-free version of the glacier CMB model is described in detail by Mölg et al. (2008, 2009, 2012). The model has been applied to simulating glaciers in a wide variety of climatic settings (e.g. Mölg et al., 2012; Collier et al., 2013; Nicholson et al., 2013; MacDonell et al., 2013). The CMB model solves the surface energy balance equation to determine the energy available for melt and other mass fluxes, given by

$$S_{\downarrow} \cdot (1 - \alpha) + \epsilon \cdot (L_{\downarrow} - \sigma \cdot T_{\text{SFC}}^4) + QS + QL + QG + QPRC = F_{\text{NET}} \quad (1)$$

where the terms correspond to, from left to right, net short- and long-wave radiation, turbulent fluxes of sensible and latent heat, the ground heat flux (composed of conduction and penetrating shortwave radiation) and the heat flux from precipitation. Following the convention in mass balance modelling, fluxes are defined as positive when energy transfer is to the surface. The residual energy flux, F_{NET} , constitutes

the energy available for melt provided the surface temperature has reached the melting point. The specific mass balance is calculated from solid precipitation, surface vapour fluxes, surface and subsurface melt, and refreeze of liquid water in the snowpack. Surface vapour fluxes (M_v ; i.e., sublimation or deposition [kg m^{-2}] depending on the sign of QL) at each time step Δt are calculated according to

$$M_v = \frac{QL \cdot \Delta t}{L_H} \quad (2)$$

where L_H is the latent heat of sublimation ($2.84 \times 10^6 \text{ J kg}^{-1}$) or vapourization ($2.51 \times 10^6 \text{ J kg}^{-1}$), depending on the surface temperature. The CMB model treats numerous additional processes, including the evolution of surface albedo and roughness based on snow depth and age; snowpack compaction and densification by refreeze; and the influence of penetrating solar radiation, refreeze and conduction on the near-surface englacial temperature distribution. Physical parameter values for snow and ice are provided in Table 1.

2.2 Inclusion of debris

For this study, the glacier CMB model was modified to include a treatment for supraglacial debris according to two cases: (1) one with no treatment of moisture fluxes or phase changes in the debris layer, congruent with previous studies (CMB-DRY), and (2) one that introduces a reservoir to parameterize the moisture content of the debris layer and its phase, and also includes a latent heat flux calculation (CMB-RES). The simulations are performed as point simulations, due to the availability of both meteorological-forcing and evaluation data at a single location.

2.2.1 Surface temperature

Consistent with previous modelling studies of debris-covered glaciers (e.g. Nicholson and Benn, 2006; Reid and Brock, 2010; Reid et al., 2012; Zhang et al., 2011), the model employs an iterative approach to prognosing surface temperature, with the solution yielding zero residual flux in the surface energy balance (Eq. 1). The model uses the Newton-Raphson method to calculate T_{SFC} at each time step, as implemented in Reid and Brock (2010), with a different termination criteria of $|F_{\text{NET}}| < 1 \times 10^{-3}$. When snow or ice are exposed at the surface, the resulting T_{SFC} is reset to the melting point if it exceeds this value, and energy balance closure is achieved by using the residual energy for surface melt.

2.2.2 Subsurface temperature

Both versions of the CMB model prognose the temperature distribution in the upper subsurface following the conservation of energy. The vertical levels selected for the case study in Sect. 2.3 are defined in Table 2, and are set at fixed depths in the subsurface, from 0.0 to 9.0 m, that track the glacier

surface as it moves due to mass loss or gain. On this grid, the 1-D heat equation becomes

$$\rho c \frac{dT}{dt} = \rho c \frac{\partial T}{\partial t} = \frac{\partial}{\partial z} \left(k \frac{\partial T}{\partial z} \right) + \frac{\partial Q}{\partial z} \quad (3)$$

where ρ is the density [kg m^{-3}]; c is the specific heat capacity [$\text{J kg}^{-1} \text{K}^{-1}$]; T is the englacial temperature [K]; k is the thermal conductivity [$\text{W m}^{-1} \text{K}^{-1}$]; and Q is the heat flux due to non-conductive processes (penetrating shortwave radiation) [W m^{-2}].

For these simulations, the numerical scheme used to solve Eq. (3) was updated from a centred-difference approach to a Crank–Nicolson scheme, which was solved following Smith (1985). The greater stability of the numerics permits the subsurface layer spacing to be decreased to 1 cm throughout the debris from ~ 10 cm previously. The vertical grid spacing is thus consistent with the small number of previous studies that explicitly simulate heat conduction in the debris (Reid and Brock, 2010; Reid et al., 2012; Lejeune et al., 2013), rather than assume that the temperature gradient is approximately linear. The convergence of the numerical solution down to a vertical grid spacing of 1 mm was checked; however, the results did not strongly differ from the 1-cm case.

With the exception of Lejeune et al. (2013), the ice temperature in previous modelling studies has been assumed to be at the melting point, due to the focus on the ablation season (e.g. Nicholson and Benn, 2006; Reid and Brock, 2010). Although this assumption has been validated by field measurements (e.g. Conway and Rasmussen, 2000; Brock et al., 2010), it limits the temporal applicability of the model and may contribute to the overestimation of night-time surface temperatures when the overlying air temperature drops below the melting point (Reid and Brock, 2010). The CMB models explicitly simulate heat conduction throughout the glacier column. Therefore, the ice temperature is a prognostic variable at all levels except the bottom boundary, where a zero-flux condition is imposed. Finally, subsurface heating due to penetrating shortwave radiation is not considered when glacier debris is exposed at the surface (e.g. Reid and Brock, 2010).

2.2.3 Physical and thermal properties

The important physical properties of the glacier subsurface in Eq. (3) – density ρ , thermal conductivity k , and specific heat capacity c – are non-uniform with depth. Defining m_s and m_d as the levels corresponding to the bottom of the snowpack and debris layers (cf. Fig. 1), respectively, the column properties (generalized as $f(z)$) are specified as

$$f(z) = \begin{cases} f_{\text{snow}} & z \leq m_s \\ f_{\text{deb}} & m_s < z \leq m_d \\ f_{\text{ice}} & z > m_d \end{cases} \quad (4)$$

Standard values are selected for snow and glacial ice properties (Table 1), with the exception of snow density, which is a prognostic variable. Within the debris layer, the properties of each 1-cm layer are a weighted average of the depth-invariant whole-rock values, f_{wr} , and the content of the pore space, f_{ϕ} , as determined by an assumed linear porosity function, ϕ

$$f_{\text{deb}}(z) = \phi(z) \cdot f_{\phi}(z) + (1 - \phi(z)) \cdot f_{\text{wr}} \quad (5)$$

For CMB-DRY, the debris pore space contains only air ($f_{\phi} = f_{\text{air}}$), while the weighted average in CMB-RES also considers the bulk water and ice content of the debris of saturated layers. The porosity function is discussed further in Sect. 2.3.

2.2.4 Moisture in the debris layer

For CMB-DRY, rainfall or other liquids water inputs are instantaneously removed as runoff from the debris layer and do not accumulate or contribute to vapour exchanges between the debris and the atmosphere, similar to previous modelling studies (e.g. Reid and Brock, 2010; Reid et al., 2012; Lejeune et al., 2013).

For CMB-RES, a reservoir is introduced for moisture accumulation and phase changes (Fig. 1). The reservoir depth for each column is calculated as the sum of the debris porosity over the debris thickness. Thus, the pore space in the debris is represented as a single reservoir, rather than treating the storage in each 1-cm layer individually. Liquid water, from rainfall or melt of the overlying snowpack, instantly infiltrates the reservoir. The location of the water and/or ice in the debris is not prognosed; rather, moisture is assumed to occupy the lowest debris layers, adjacent to the glacier ice.

In addition, when the ice-debris interface reaches the melting point, a minimum debris water content is imposed to reflect field observations of a basal saturated layer during the ablation season (e.g. Nakawo and Young, 1981; Conway and Rasmussen, 2000; Kayastha et al., 2000; Reznichenko et al., 2010; Nicholson and Benn, 2012). As the water content of glacier debris cover is poorly constrained and no measurements are available, the minimum value is set to the amount of water needed to saturate the lowest 1-cm layer in the debris, given its porosity and ice content. The horizontal drainage of debris water is accounted for using a simplistic representation of the runoff timescale, which is a linear function of terrain slope and varies from 1 to 0 h⁻¹ between 0° and 90° (Reijmer and Hock, 2008).

Congruent with the simple nature of the reservoir parameterization, the heat flux from precipitation is only applied at the surface in CMB-RES, and subsurface heat transport by water percolation is not included. This treatment is consistent with the findings of Sakai et al. (2004), namely that the heat flux due to rainfall percolation contributes minimally to sub-debris ice melt, although its influence may depend on debris permeability (Reznichenko et al., 2010).

2.2.5 Turbulent fluxes of latent and sensible heat

The turbulent fluxes of sensible heat (both models) and latent heat (CMB-RES) were computed using bulk aerodynamic formulae and corrected for atmospheric stability according to the bulk Richardson number, as is standard in glacier energy balance modelling (e.g. Braithwaite, 1995; Reid and Brock, 2010). The bulk Richardson number was constrained within reasonable limits following Fyffe et al. (2014), with the correction applied to fewer than 2.0 % of total time steps in the simulations. The latent heat flux in CMB-DRY was set to zero, to be consistent with previous studies of debris-covered glaciers, as no measurements of surface relative humidity were available. For CMB-RES, the surface vapour pressure was needed but unknown.

For the case study described in Sect. 2.3, an automatic weather station (AWS) measured relative humidity at a height of $z_{\text{air}} = 2.16$ m, from which the partial vapour pressure was calculated. The partial density of water vapour was then obtained from,

$$e_{\text{air}} = \rho_{\text{air}}^{\text{vap}} R_v T_{\text{air}} \quad (6)$$

where the symbols correspond to, from left to right, the air's water vapour partial pressure, the partial density of water vapour, the specific gas constant for water vapour (461.5 J kg⁻¹ K⁻¹), and the air temperature at a height of z_{air} . In this study, we assumed that $\rho_{\text{air}}^{\text{vap}}$ is constant between the sensor and the surface of the debris layer, i.e., that water vapour in the atmospheric surface layer is well mixed. The vapour pressure at the surface is therefore given by,

$$e_{\text{sfc}}^* = \frac{e_{\text{air}} T_{\text{sfc}}}{T_{\text{air}}} \quad (7)$$

For a completely unsaturated glacier debris layer in CMB-RES, a latent heat flux would nonetheless arise due to the vapour pressure gradient that results from the temperature difference between the surface and z_{air} . However, when water or ice are present in the debris, the final calculation of the surface vapour pressure, e_{sfc} , includes a linear correction towards the saturation value $e_{\text{sfc sat}}$ at T_{sfc} according to,

$$e_{\text{sfc}} = e_{\text{sfc}}^* + (e_{\text{sfc sat}} - e_{\text{sfc}}^*) \cdot \left(1 - \frac{\Theta_{\text{air}}}{\phi_{\text{bulk}}} \right) \quad (8)$$

where e_{sfc}^* is the initial guess in Eq. (7); Θ_{air} is the void fraction of the bulk layer that is occupied by air; and ϕ_{bulk} is the bulk debris porosity, which is invariant under different debris thicknesses due to the linear specification of ϕ (as described in Sect. 2.3). Θ_{air} is given by,

$$\Theta_{\text{air}} = \sum_{i=1}^{m_K-1} \frac{\phi_i}{N} \quad (9)$$

where m_K is the level of the saturated horizon in the debris and N is the total number of layers in the debris. When the

355 debris is completely unsaturated, $\Theta_{\text{air}} = \phi_{\text{bulk}}$, and when it is completely saturated, $\Theta_{\text{air}} = 0$.

Therefore, the surface vapour pressure in CMB-RES is a linear function of the moisture content of the reservoir rather than a wetted debris surface: as the reservoir fills from 360 infiltration of rainfall or snowmelt, the distance between the surface and the saturated horizon (represented by Θ_{air}) decreases and e_{sfc} approaches saturation.

2.2.6 Mass balance 415

The total mass balance calculation in CMB-DRY and CMB-RES accounts for the following mass fluxes [kg m^{-2}] at each time step: solid precipitation, surface and vertically integrated subsurface melt, meltwater refreeze and formation 420 of superimposed ice in the snowpack, changes in liquid water storage in the snowpack, and surface vapour fluxes. The contribution of surface vapour fluxes to or from the debris layer is zero when overlying snow cover is present and in CMB-DRY. In CMB-RES, these fluxes also contribute to changes 425 in the debris water and ice content of the reservoir. For both models, sub-debris ice melt is calculated as the vertical integral of melt in the ice column underlying the debris.

Liquid precipitation contributes indirectly to the mass balance through changes in storage in the snowpack in both 430 CMB models and directly in CMB-RES via reservoir storage. However, changes in the debris water and ice content in CMB-RES are not included in the mass balance calculation, so as to allow for a more direct comparison between CMB-RES and CMB-DRY of the influence of including the latent 435 heat flux. The impact of changes in the storage of water and ice in the debris is quantified in Sect. 3 and has a negligible influence on the total accumulated mass balance.

2.3 Miage Glacier case study 440

The study area is the Miage glacier in the Italian Alps ($45^{\circ} 47' \text{ N}$, $6^{\circ} 52' \text{ E}$; Fig. 2). This glacier was selected due to the availability of meteorological data from an automatic 390 weather station (AWS), located on the lower, debris-covered 445 part of the glacier at an elevation of 2030 m a.s.l.. The debris thickness was determined by a point measurement to be 23 cm. At the surface, the debris is composed mainly of coarse gravel and cobbles, ranging in size from a few centimetres to 25 cm, with occasional larger rocks, one to two 450 meters in size. The AWS site was deliberately chosen to be upwind from any nearby large boulders.

We perform two simulations, one for summer 2008 and one for fall 2011. The former covers the period of 25 June–11 August 2008, with the first 25 days discarded as model 400 spin-up time. For much of the 2008 simulation, the AWS provided hourly values of air temperature, vapour pressure, wind speed, and incoming short- and long-wave radiation (Fig. 3). However, during the spin-up period, wind speed and 405 incoming longwave radiation were missing due to a program-

ming error in the AWS. To provide this missing data, wind speed was generated synthetically using the hourly average from the measured data during the evaluation period. Incoming longwave radiation was obtained from the ERA-Interim reanalysis ($0.75^{\circ} \times 0.75^{\circ}$ resolution; Dee et al., 2011), using data from the closest model grid cell after interpolation from 12 hourly to hourly reference points. For the time period where both ERA Interim and AWS data overlap (20 July–11 August 2008), the mean deviation (MD) and mean absolute deviation (MAD; ERA minus AWS) are ~ 13 and $\sim 35 \text{ W m}^{-2}$, which likely arises due to the difference between modelled and real terrain height of -450 m . Lastly, a rain gauge was not installed at the AWS site in 2008. We therefore used input data from another AWS located 4 km away (denoted as AWS2 in Fig. 2) and assumed that they were representative of conditions at the AWS on the Miage glacier.

The 2008 simulation is intended to coincide with a supplementary field measurement program. Between 20 July and 11 August, surface temperature and the turbulent fluxes of latent and sensible heat were measured. The first field was measured with a CNR1 radiation sensor (Kipp & Zonen, Delft, the Netherlands), while the latter two fluxes were measured by an eddy covariance (EC) station. This comprised a CSAT three-dimensional sonic anemometer and KH2O Krypton Hygrometer (both Campbell Scientific Limited, Shephed, UK), installed at a height of 2 m above the debris surface. These sensors measured the three components of turbulent wind velocity, virtual temperature and water vapour concentrations at an interval of 50 ms. Raw data were processed using Campbell Scientific OPEC software, which included a “WPL” correction for density effects (Webb et al., 1980) and 30-min averages of the 50-ms scans were stored. The data were filtered for outliers using three times their standard deviation before being used for evaluation (Brock et al., 2010). Surface temperature was calculated from the upwelling longwave radiation recorded by the CNR1, using an emissivity of 0.94. The AWS tripod provided a stable platform on the slowly melting glacier surface, although the possibility of tilting of the instrument mast cannot be avoided. These measurements provide a unique dataset with which to evaluate the CMB models using direct measurement of turbulence in the surface atmospheric layer above a debris-covered glacier.

However, the 2008 simulation does not contain any phase changes, since the air temperature remained above freezing (cf. Fig. 3a). In order to fully demonstrate the model capabilities, we performed a second simulation from 6 June–11 October 2011, discarding all but the period of 14 September–11 October as model spin-up time, due to the focus on the influence of phase changes. We focused our analysis on two freezing events, from 18–19 September and 7–9 October 2011. Incoming long-wave radiation, precipitation and mean wind speed were available hourly from the AWS (forcing data not shown), and measured surface temperature data, esti-

460 mated from the upwelling longwave radiation recorded by 515
the CNR1, were available for model evaluation.

A final forcing variable for the calculation of the debris
surface energy balance, surface pressure, was missing for
both the 2008 and 2011 simulations. These data were ob-
465 tained from the ERA Interim reanalysis, at 6 hourly temporal
resolution, and again from the closest grid cell. A correc-
tion was applied for the difference between the real and mod-
elled terrain height using the hypsometric equation, assuming
a linear temperature gradient calculated from the AWS and 520
470 the air temperature on the first model level in ERA interim.
For both simulations, the same subsurface layer spacing was
used and is provided in Table 2. The englacial temperature
profile was initialized at the melting point, since the simu-
475 lations both began in June. Uncertainties in the temperature
initialization were addressed by the inclusion of long spin-up
periods.

For both CMB-DRY and CMB-RES, we assumed that the
debris porosity is a linear function of depth in the debris,
decreasing from 40 % at the surface down to 20 % at the 530
480 debris-ice interface. A range of 19 – 60 % percent void space
by volume was measured on the Miage glacier, by placing a
known volume of surface debris in a graduated bucket and
measuring the volume of water required to fill the air spaces
485 (Brock et al., 2006). For this study, we used an upper-bound
of 40 %, such that the bulk porosity (30 %) was consistent
with other reported values for glacier debris (Nicholson and
Benn, 2012). A sensitivity study using the measured upper
490 bound of 60 % showed that while sub-debris ice melt was
strongly affected (it decreased by $\sim 17\%$ in both simula-
495 tions), the CMB model behaviour and the main results pre-
sented in Sect. 3 remained intact. Other physical and thermal
properties of the column were either taken from field mea-
surements or specified from values used in previous mod-
elling studies of this glacier (e.g. Reid and Brock, 2010). The
500 porosity value of 20 % in the lowest 1-cm layer in the debris 545
gave a minimum water content of 2 kg m^{-2} that was imposed
only when the sub-debris ice was at the melting point. Sub-
debris ice melt changes by $\pm 1.8\%$ if the minimum value is
removed or doubled in the 2008 simulation.

A slope of 7° at the AWS gives a runoff timescale of 500
 0.92 h^{-1} . This simple representation of runoff timescales
does not consider contributions from upslope regions in the
glacier; however, we feel that this is an appropriate first step
given that horizontal transport of water within the debris is
505 poorly constrained and no measurements are available. Vary-
ing the runoff timescale by $\pm 4\%$ (equivalent to changing the
slope from 4° to 10°) results in small changes in total ac-
cumulated mass balance and sub-debris ice melt during the
summer 2008 simulation, of less than ± 0.6 and $\pm 0.4\%$, re-
510 spectively. The results in the transition season of fall 2011 560
are more sensitive, with changes in these variables of up to
 ± 1.0 and $\pm 2.0\%$, respectively.

Finally, although the CMB models are evaluated against
a short summer period in 2008 and in fall 2011, they are ap-

plicable throughout the annual cycle and to glaciers of any
temperature regime, as illustrated in Fig. 1.

3 Results

3.1 Comparison with in situ measurements

The surface temperatures (T_{sfc}) simulated by CMB-DRY and
CMB-RES are in good agreement with measurements for
both the 2008 and 2011 simulations (Fig. 4a and d; Ta-
ble 3). The models tend to underestimate daily maximum
temperatures in 2008 and night-time radiative cooling in
2011, respectively. However, for both simulations, the mod-
els reproduce the diurnal cycle and its variability well. The
CMB models also capture the variability of the sensible
heat flux (QS), but the simulated magnitude of heat trans-
fer to the overlying atmosphere is greater than reported by
the EC station (Fig. 4b). The overestimation of QS for the
CMB-DRY run is in part attributable to the lack of latent
heat flux (QL), which means that an average energy loss of
 $\sim 24 \text{ W m}^{-2}$ is not captured (Fig. 4c, cf. Table 3). CMB-
RES has a greatly reduced but still non-negligible bias in
QS, again, in part, because evaporative cooling is underesti-
mated, by $\sim 6 \text{ W m}^{-2}$. The smaller simulated latent heat flux
compared with the EC data results from the approach used to
estimate surface vapour pressure (cf. Sect. 2.2), which pro-
duces an average gradient of only -0.5 hPa m^{-1} between
the surface and overlying air (Fig. 5a).

3.2 Modelling insights from the 2008 simulation

In total, the influence of the reservoir parameterization on
the accumulated mass balance between 20 July and 11 Au-
gust 2008 is small, increasing from -241.0 kg m^{-2} in CMB-
DRY to -250.6 kg m^{-2} in CMB-RES (Fig. 5b). These val-
ues are equivalent to an ablation rate of approximately
 $11 \text{ mm w.e. d}^{-1}$, which is in order of magnitude agreement
with the value of $22 \text{ mm w.e. d}^{-1}$ reported by Fyffe et al.
(2012) for the Miage glacier, based on the entire ablation sea-
sons of 2010 and 2011.

The mass fluxes underlying the simulated mass balance
signal are determined by the surface energy balance, whose
daily-mean components are shown in Fig. 6a for CMB-
RES. Energy receipt mainly through net shortwave radia-
tion is generally counteracted by energy losses through net
longwave radiation, heat conduction (QC), and the turbulent
fluxes of latent (QL) and sensible (QS) heat. The heat flux
to the debris surface from precipitation (QPRC) has an aver-
age value of -12.5 W m^{-2} during rainfall events. However,
since the precipitation temperature is assumed to be the same
as T_{air} , QPRC is a stronger energy sink for daytime rainfall.
These energy fluxes produce ablation that is dominated by
sub-debris ice melt and evaporation over the evaluation pe-
riod (Fig. 6b; Table 4). Surface melt, refreeze, sublimation
and deposition are zero, since there is no solid precipitation

and both the debris surface and internal temperatures remain above the melting point.

Compared with CMB-DRY, CMB-RES simulates slightly lower daytime debris-surface temperatures, as a result of heat extraction by QL (cf. Fig. 4a, Table 3). Energy transfer to the debris-ice interface is therefore also lower, contributing to a small reduction in sub-debris ice melt, of 7.5 kg m^{-2} (Table 4). However, the reduction in melt is more than compensated by surface vapour fluxes, with a total of 17.3 kg m^{-2} of evaporation over the evaluation period. Evaporation dominates during the day (95 % of the total), while smaller amounts of condensation occur mainly at night (64 %) or in the early morning.

Water accumulates in the supraglacial debris after rainfall events and is then removed, mainly by horizontal drainage but also by evaporation (Fig. 7). The total accumulated mass balance is negligibly altered if changes in debris water content are considered in addition to surface vapour fluxes. Both models treat the physical properties of the debris layer – thermal conductivity, density, and specific heat capacity – as functions of depth. Figure 8a–c shows their variation with depth for “dry” conditions, when there is no significant debris water storage, and for “wet” conditions, when there is significant water present, as a result of rainfall. “Dry” conditions prevail, comprising 76 % of the evaluation period (Fig. 8d–f), under which, as the porosity decreases with depth, the debris thermal conductivity and density increase while the specific heat capacity decreases. The debris physical properties in CMB-DRY and CMB-RES are the same, with the exception of the bottom layer adjacent to the debris-ice interface, which remains fully saturated as a result of the moisture source term described in Sect. 2.2. Water present in this layer acts to increase all three properties compared with CMB-DRY. Rainfall events and the associated moisture storage extend this influence upwards through the debris layer, with a significant alteration to the fully saturated layers (spanning the depth between 20 and 23 cm for the “wet” sample time slice) and a smaller effect on the partially saturated layer (at a depth of 19 cm). The debris specific heat capacity is the most strongly affected physical property, since the value of water is approximately four times that of air ($4181 \text{ vs. } 1005 \text{ J kg}^{-1} \text{ K}^{-1}$).

The effective thermal diffusivity of the debris is inversely proportional to the specific heat capacity and the debris density. Increases in both of these quantities, but particularly in the former, reduce heat diffusion over affected layers compared with CMB-DRY. Therefore, in combination with heat extraction by QL, the change in subsurface physical properties reduces the amplitude and depth-penetration of the diurnal temperature cycle in the debris layer (Fig. 9). Fluctuations in the magnitude of QL have a correlation coefficient of 0.78 with the temperature difference between CMB-RES and CMB-DRY in the top 6 cm of the debris, while reductions in the effective thermal diffusivity have a correlation coefficient of 0.6 with the temperature difference in the bottom 6 cm.

3.3 Impact of phase changes in the 2011 simulation

Two freezing events occur during the 2011 simulation, between 18 September 23:00 LT–19 September 14:00 LT and between 7 October 9:00 LT–9 October 9:00 LT, at the tail end of two precipitation events with sub-zero air temperatures (cf. Fig. 4d). Net longwave and shortwave radiation are reduced, due to cooler surface temperatures and to small amounts of snowfall that increase the surface albedo (Fig. 10a). Rapid melt of the thin overlying snow cover ($< 0.5 \text{ cm}$) and infiltration of rainfall at the beginning of the precipitation events provide the source water for refreeze in the debris (Figs. 10b and 11a). During the first event, a maximum of 1.0 kg m^{-2} of ice is produced, which persists in the basal debris layer for a further three days after the last time step with refreeze. In the second event, the debris ice content reaches 1.4 kg m^{-2} , and does not melt away before the end of the simulation.

The bulk presence of liquid water and ice in the debris layer influences the vertical temperature profile in two competing ways (Fig. 11b–d). Latent heat release due to refreezing warms the subsurface, on average by 0.3 K but exceeding 0.7 K for the hourly time steps with the greatest refreeze. However, the presence of ice in saturated basal layers constrains the debris temperature to the melting point. In combination with a reduction in the effective thermal diffusivity of saturated layers, the modulation of debris temperature results in a decrease in sub-debris ice melt of 7.0 % in CMB-RES compared with CMB-DRY.

The accumulated mass balance between 14 September–11 October 2011 is -172.4 kg m^{-2} for CMB-DRY and -168.8 kg m^{-2} for CMB-RES. Changes in water and ice storage again have a negligible impact on simulated mass balance, resulting in a further ablation of 0.2 kg m^{-2} . Thus, for the fall transition season, surface vapour fluxes do not compensate for the reduction in sub-debris ice melt due to the thermodynamic influence of ice in the debris. However, considering the same summer period in 2011 as in 2008 (20 July–11 August), the percent changes in accumulated mass balance and sub-debris ice melt are +4.0 % and –3.2 %, respectively, consistent with the findings of the 2008 simulation. Therefore, the influence of the reservoir parameterization varies seasonally.

4 Discussion

Both the observed and simulated QL are non-zero over the simulation period, with regular fluctuations on the order of 10 W m^{-2} and occasional spikes of more than $\pm 100 \text{ W m}^{-2}$ (after filtering, as described in Sect. 2.3; cf. Fig. 4c). Among other sources of error, intense precipitation can cause erroneous spikes in the EC measurements, as a result of raindrops interfering with the path of the sonic anemometer (e.g. Aubinet et al., 2012). However, of the 15 occurrences of

670 spikes greater than $\pm 100 \text{ W m}^{-2}$ in the EC data, only two
 occur during or within one hour of precipitation. In com- 725
 bination with previously reported large QL values, of up to
 -800 W m^{-2} during rainfall events on heated debris (Brock
 et al., 2010), neglecting QL in a surface energy balance cal-
 675 culation can be inappropriate, and under certain meteorolog-
 ical conditions is likely to have a significant impact on the 730
 calculated energy fluxes.

The difference in accumulated mass balance between
 CMB-RES and CMB-DRY is relatively small, for a point
 680 application in this configuration. However, the daily mean
 evaporation rate was $\sim 0.9 \text{ mm w.e.}$ in 2008 (June to early 735
 August) and $\sim 0.6 \text{ mm w.e.}$ in 2011 (June to September),
 which is comparable to values reported for clean glaciers
 (e.g. Kaser, 1982). Scaled up to a larger debris-covered area,
 685 evaporation would represent a significant mass flux. Further-
 more, the presence of debris ice, even in small amounts, 740
 has an important thermodynamic influence by suppressing
 sub-debris ice melt, with implications for dry simulations of
 debris-covered glaciers in or close to transition seasons.

690 The simulated QL and surface vapour fluxes depend on the
 estimate of the surface vapour pressure, which is an impor- 745
 tant source of uncertainty in the CMB-RES model. In unsatu-
 rated soil sciences, the relative humidity is often treated as an
 exponential function of the liquid water pressure in the pore
 695 space using the thermodynamic relationship of Edlefsen and
 Anderson (1943) (e.g. Wilson et al., 1994; Karra et al., 2014). 750
 However, testing an exponential relationship with the mois-
 ture content of the debris in CMB-RES resulted in strong bi-
 ases in QL ($\text{MD} = 28$; $\text{MAD} = 96 \text{ W m}^{-2}$) and a shift from
 700 QL as an energy sink to a gain, which was inconsistent with
 the EC data. For simplicity, we employed a linear approach, 755
 and there may be some support for this treatment in coarser
 texture soil, as Yeh et al. (2008) found that the effective de-
 gree of saturation in sand decreased approximately linearly
 705 in the top two meters above the water table.

In reality, water vapour fluxes occur at the saturated hori- 760
 zon, either at the surface or within the debris layer. However,
 in the 2008 simulation, the mean depth of the saturated hori-
 710 zon was 21.5 cm, where the proximity of glacier ice damped
 temperature fluctuations and constrained the mean tempera-
 ture to $\sim 275 \text{ K}$. Therefore, computing vapour fluxes at this 765
 level produced a very small latent heat flux, of -3.1 W m^{-2}
 on average, that was also not in agreement with the EC data.
 CMB-RES likely provides an underestimate of the simulated
 715 location of the saturated horizon, since capillary action was
 not taken into account. For fine gravel soils (grain size of 2–770
 5 mm), capillary rise is on the order of a few cm (Lohman,
 1972), while for coarser, poorly sorted glacier debris, the ef-
 fect may be smaller. Underestimation of the height of the
 720 saturated horizon, and therefore of both the debris tempera-
 ture and the saturation vapour pressure, is consistent with 775
 the small latent heat flux when vapour fluxes are computed
 at this level. As a part of future work, there is a need to accu-

rately compute the vapour fluxes at the level of the saturated
 horizon.

In addition to neglecting capillary action, CMB-RES also
 does not account for many internal physical processes that
 have been highlighted in unsaturated soil sciences, includ-
 ing water vapour flow due to gradients in concentration and
 temperature; liquid water flow in response to hydraulic gra-
 dients; volume changes due to changes in the degree of sat-
 uration (e.g. Sheng, 2011); deposition of water vapour and
 its contribution to the formation of thin ice lenses (e.g. Karra
 et al., 2014); and heat or moisture advection as a result of air-
 flow (e.g. Zeng et al., 2011). However, incorporation of these
 processes into CMB-RES is currently limited by a lack of
 appropriate evaluation data. Instead, we focus on including
 processes related to phase changes, which have been demon-
 strated to have an impact on the subsurface temperature field
 and ablation rate (Reznichenko et al., 2010; Nicholson and
 Benn, 2012). As a part of future work, CMB-RES could be
 improved by distinguishing the location of debris ice and
 water separately within saturated layers, thus potentially im-
 proving the simulated debris temperature profiles as the melt-
 ing point constraint would only be applied to saturated layers
 containing ice.

The magnitude of QS is sensitive to the choice of debris
 thickness, which was selected to be 0.23 m in this study
 based on a point measurement. However, the turbulent fluxes
 measured by the EC station respond to a larger area, with
 a variable and unknown debris thickness that likely ranges
 between 20–30 cm. The agreement between measured and
 modelled QS in 2008 is improved if the debris thickness in
 the models is reduced slightly. For example, using a thick-
 ness of 20 cm reduces the MD and the MAD by $\sim 7 \text{ W m}^{-2}$,
 for both model versions. Investigating additional causes of
 discrepancies between modelled QS and that measured by
 the EC is not directly related to the inclusion of moisture in
 CMB-RES and is reserved for future work.

There are no ablation measurements available for either
 of the two simulation periods. To examine the general be-
 haviour of the CMB models, the 2008 simulation was re-
 peated with debris thicknesses of 1 to 20 cm, holding the
 sub-debris ice depth constant and scaling the minimum de-
 bris water content as 3 % of the reservoir capacity (consis-
 tent with the 23-cm simulation; Fig. 12). Total column melt
 is suppressed for all debris thicknesses compared with the
 clean-ice melt rate, with less melt in CMB-RES than CMB-
 DRY due to heat extraction by QL and the reduced thermal
 diffusivity discussed in Sect. 3.2. Therefore, the CMB mod-
 els do not reproduce the typical Østrem curve, wherein melt
 is enhanced below a critical debris thickness that ranges be-
 tween 1.5–5 cm (e.g. Loomis, 1970; Fujii, 1977; Inoue and
 Yoshida, 1980; Mattson et al., 1993) and suppressed above
 this value. The rising limb of the Østrem curve is not repro-
 duced for several reasons. First, in the clean-ice and thinly
 debris-covered simulations, lower night-time air tempera-
 tures in the beginning of the evaluation period (20–24 July

2008; cf. Fig. 4a) produce freezing events that cool the sub-
 surface. Averaged over the entire evaluation period, a non-
 negligible amount of energy is expended to warm the ice
 column as a result. For example, in the clean-ice simula-
 tion, this heat flux amounts to 3.7 W m^{-2} . For CMB-RES
 (CMB-DRY) with debris thicknesses of 1 and 2 cm, the av-
 erage energy required is 4.4 (5.3) and 3.1 (3.5) W m^{-2} , re-
 spectively. In addition, sub-zero englacial temperatures in
 the clean-ice simulation are eradicated more quickly, since
 penetrating shortwave radiation is considered. Finally, other
 processes that are not treated in the CMB models may be
 important to fully reproduce the rising limb of the Østrem
 curve, such as (1) changes in the surface albedo as the debris
 cover becomes more continuous, as in the albedo “patchi-
 ness” scheme introduced by Reid and Brock (2010), and (2)
 wind-driven evaporation inside the debris layer (Evatt et al.,
 working paper, 2014).

5 Conclusions

In this paper, we introduced a new model for the surface en-
 ergy balance and CMB of debris-covered glaciers that in-
 cludes surface vapour fluxes and a reservoir parameteriza-
 tion for moisture infiltration and phase changes. Although
 the parameterization is a simplification of the complex moist
 physics of debris, our model is a novel attempt to treat mois-
 ture within glacier debris cover, and one that permits two im-
 portant advances: (1) it incorporates the effects of ice and
 water on the physical and thermal properties of the debris
 and therefore on ice ablation, and (2) it includes an estimate
 of the moisture exchanges between the surface and the atmo-
 sphere.

The inclusion of the water vapour flux opens up avenues
 of future research. For example, distributed simulations are
 required to most rigorously investigate relevant scientific
 questions about debris-covered glaciers, such as projecting
 their behaviour and runoff under changing climate condi-
 tions. A key constraint in performing such simulations is
 obtaining forcing data, since the highly heterogeneous sur-
 face of debris-covered glaciers makes the spatial distribu-
 tion of air temperature and winds uncertain. Current ap-
 proaches, employing elevation-based extrapolation, appear
 to be inadequate (Reid et al., 2012). Interactive coupling
 with a high-resolution atmospheric model provides one so-
 lution; however, the conventional modelling approach would
 introduce errors due to the absence of moisture exchange be-
 tween the surface and the atmosphere. In incorporating that
 flux, CMB-RES is a step towards more precisely computing
 glacier-atmosphere feedbacks within coupled surface-and-
 atmosphere modelling schemes and more accurately predict-
 ing alterations in freshwater budgets and other potential im-
 pacts of glacier change.

Acknowledgements. E. Collier was supported by a Natural Sci-
 ences and Engineering Research Council of Canada (NSERC)
 CGS-D award and an Alberta Ingenuity Graduate Student Schol-
 arship. L. I. Nicholson was supported by an Austrian Science Fund
 (FWF) Elise Richter Award (#V309-N26). F. Maussion acknowl-
 edges support from the WET project (code 03G0804A), financed by
 the German Federal Ministry of Education and Research (BMBF).
 A. B. G. Bush acknowledges support from NSERC and from the
 Canadian Institute for Advanced Research. We also thank the Aosta
 Valley Autonomy Region for supplying meteorological data for the
 Lex Blanche station and P. Zöll for designing Fig. 1. We thank re-
 viewers T. Reid and G. Evatt for their helpful comments, which
 greatly improved the CMB models and this manuscript.

References

references

- Aubinet, M., Vesala, T., and Papale, D. (Eds.): *Eddy Covariance: a Practical Guide to Measurement and Data Analysis*, Springer, Dordrecht, Heidelberg, London, New York, 1–19, 2012.
- Bhambri, R., Bolch, T., Chaujar, R. K., and Kulshreshtha, S. C.: Glacier changes in the Garhwal Himalaya, India, from 1968 to 2006 based on remote sensing, *J. Glaciol.*, 57, 543–556, 2011.
- Bolch, T., Buchroithner, M., Pieczonka, T., and Kunert, A.: Planimetric and volumetric glacier changes in the Khumbu Himal, Nepal, since 1962 using Corona, Landsat TM and ASTER data, *J. Glaciol.*, 54, 592–600, 2008.
- Braithwaite, R. J.: Aerodynamic stability and turbulent sensible-heat flux over a melting ice surface, the Greenland ice sheet, *J. Glaciol.*, 41, 562–571, 1995.
- Brock, B., Mihalcea, C., Citterio, M., D’Agata, C., Cutler, M., Diolaiuti, G., Kirkbride, M. P., Maconachie, H., and Smiraglia, C.: Spatial and temporal patterns of thermal resistance and heat conduction on debris-covered Miage Glacier, Italian Alps, *Geophysical Research Abstracts, European Geosciences Union General Assembly, Vienna, Austria, 2–7 April 2006, Vol. 8, ISSN: 1029-7006*, 2006.
- Brock, B. W., Mihalcea, C., Kirkbride, M. P., Diolaiuti, G., Cutler, M. E., and Smiraglia, C.: Meteorology and surface energy fluxes in the 2005–2007 ablation seasons at the Miage debris-covered glacier, Mont Blanc Massif, Italian Alps. *J. Geophys. Res.*, 115, D09106, doi:<http://dx.doi.org/10.1029/2009JD013224>, 2010.
- Collier, E., Mölg, T., Maussion, F., Scherer, D., Mayer, C., and Bush, A. B. G.: High-resolution interactive modelling of the mountain glacier–atmosphere interface: an application over the Karakoram, *The Cryosphere*, 7, 779–795, doi:<http://dx.doi.org/10.5194/tc-7-779-2013>, 2013.
- Conway, H. and Rasmussen, L. A.: Summer temperature profiles within supraglacial debris on Khumbu Glacier, Nepal, *Debris-Covered Glaciers, IAHS PUBLICATION no. 264*, 89–97, 2000.
- Dall’Amico, M., Endrizzi, S., Gruber, S., and Rigon, R.: A robust and energy-conserving model of freezing variably-saturated soil, *The Cryosphere*, 5, 469–484, doi:<http://dx.doi.org/10.5194/tc-5-469-2011>, 2011.

- Dee, D. P., Uppala, S. M., Simmons, A. J., Berrisford, P., Poli, P., Kobayashi, S., Andrae, U., Balmaseda, M. A., Balsamo, G., Bauer, P., Bechtold, P., Beljaars, A. C. M., van de Berg, L., Bidlot, J., Bormann, N., Delsol, C., Dragani, R., Fuentes, M., Geer, A. J., Haimberger, L., Healy, S. B., Hersbach, H., Hlm, E. V., Isaksen, L., Källberg, P., Köhler, M., Matricardi, M., McNally, A. P., Monge-Sanz, B. M., Morcrette, J.-J., Park, B.-K., Peubey, C., de Rosnay, P., Tavolato, C., Thpaut, J.-N., and Vitart, F.: The ERA-Interim reanalysis: configuration and performance of the data assimilation system, *Q. J. Roy. Meteor. Soc.*, 137, 553–597, 2011.
- Edlefsen, N. E. and Anderson, A. B. C.: Thermodynamics of soil moisture, *Hilgardia*, 15, 31–298, 1943.
- Foster, L. A., Brock, B. W., Cutler, M. E. J., and Diotri, F.: A physically based method for estimating supraglacial debris thickness from thermal band remote-sensing data, *J. Glaciol.*, 58, 677–691, 2012.
- Fujii, Y.: Experiment on glacier ablation under a layer of debris cover, *J. Japan. Soc. Snow Ice (Seppy)*, 39, 20–21, 1977.
- Fyffe, C., Brock, B. W., Kirkbride, M. P., Mair, D. W. F., and Diotri, F.: The hydrology of a debris-covered glacier, the Miage Glacier, Italy, BHS Eleventh National Symposium, Hydrology for a changing world, Dundee, 9–11 July 2012, doi:<http://dx.doi.org/10.7558/bhs.2012.ns1910.7558/bhs.2012.ns19>, 2012.
- Fyffe, C., Reid, T. D., Brock, B. W., Kirkbride, M. P., Diolaiuti, G., Smiraglia, C., and Diotri, F.: A distributed energy balance melt model of an alpine debris-covered glacier, *J. Glaciol.*, in press, 2014.
- Han, H. D., Ding, Y. J., and Liu, S. Y.: A simple model to estimate ice ablation under a thick debris layer, *J. Glaciol.*, 52, 528–536, 2006.
- Inoue, J. and Yoshida, M.: Ablation and heat exchange over the Khumbu Glacier, *J. Japan. Soc. Snow Ice (Seppy)*, 39, 7–14, 1980.
- Kääb, A., Berthier, E., Nuth, C., Gardelle, J., and Arnaud, Y.: Contrasting patterns of early twenty-first-century glacier mass change in the Himalayas, *Nature*, 488, 495–498, 2012.
- Karra, S. and Painter, S. L. and Lichtner, P. C.: Three-phase numerical model for subsurface hydrology in permafrost-affected regions, *The Cryosphere Discussions*, 8, 149–185, doi:<http://dx.doi.org/10.5194/tcd-8-149-201410.5194/tcd-8-149-2014>, 2014.
- Kaser, G.: Measurement of evaporation from snow, *Arch. Met. Geoph. Biokl. Ser. B.*, 30, 333–340, 1982.
- Kayastha, R. B., Takeuchi, Y., Nakawo, M., and Ageta, Y.: Practical prediction of ice melting beneath various thickness of debris cover on Khumbu Glacier, Nepal using a positive degree-day factor, Symposium at Seattle 2000 – Debris-Covered Glaciers, IAHS Publ., 264, 71–81, 2000.
- Klok, E. J., and Oerlemans, J.: Model study of the spatial distribution of the energy and mass balance of Morteratschgletscher, Switzerland, *J. Glaciol.*, 48, 505–518, 2002.
- Kraus, H.: An energy-balance model for ablation in mountainous areas, *Snow and Ice-Symposium-Neiges et Glaces*, August 1971, IAHS-AISH PUBLICATION no. 104, 1975.
- Lejeune, Y., Bertrand, J.-M., Wagnon, P., and Morin, S.: A physically based model of the year-round surface energy and mass balance of debris-covered glaciers, *J. Glaciol.*, 59, 327–344, doi:<http://dx.doi.org/10.3189/2013JoG12J14910.3189/2013JoG12J149>, 2013.
- Lohman, S. W.: Ground-water hydraulics. U.S. Geological Survey Professional Paper 708, 1972.
- Loomis, S. R.: Morphology and ablation processes on glacier ice, *Assoc. Am. Geogr. Proc.*, 2, 88–92, 1970.
- MacDonell, S., Kinnard, C., Mölg, T., Nicholson, L., and Abermann, J.: Meteorological drivers of ablation processes on a cold glacier in the semi-arid Andes of Chile, *The Cryosphere*, 7, 1513–1526, doi:<http://dx.doi.org/10.5194/tc-7-1513-201310.5194/tc-7-1513-2013>, 2013.
- Mattson, L. E., Gardner, J. S., and Young, G. J.: Ablation on debris covered glaciers: an example from the Rakhiot Glacier, Punjab, Himalaya, *Snow and Glacier Hydrology*, IAHS-IASH Publ., 218, 289–296, 1993.
- Mölg, T., Cullen, N. J., Hardy, D. R., Kaser, G., and Klok, E. J.: Mass balance of a slope glacier on Kilimanjaro and its sensitivity to climate, *Int. J. Climatol.*, 28, 881–892, 2008.
- Mölg, T., Cullen, N. J., Hardy, D. R., Winkler, M., and Kaser, G.: Quantifying climate change in the tropical midtroposphere over East Africa from glacier shrinkage on Kilimanjaro, *J. Climate*, 22, 4162–4181, 2009.
- Mölg, T., Maussion, F., Yang, W., and Scherer, D.: The footprint of Asian monsoon dynamics in the mass and energy balance of a Tibetan glacier, *The Cryosphere*, 6, 1445–1461, doi:<http://dx.doi.org/10.5194/tc-6-1445-201210.5194/tc-6-1445-2012>, 2012.
- Nakawo, M. and Young, G. J.: Field experiments to determine the effect of a debris layer on ablation of glacier ice, *Ann. Glaciol.*, 2, 85–91, 1981.
- Nakawo, M. and Young, G. J.: Estimate of glacier ablation under a debris layer from surface temperature and meteorological variables, *J. Glaciol.*, 28, 29–34, 1982.
- Nicholson, L. and Benn, D.: Calculating ice melt beneath a debris layer using meteorological data, *J. Glaciol.*, 52, 463–470, 2006.
- Nicholson, L. and Benn, D.: Properties of natural supraglacial debris in relation to modelling sub-debris ice ablation, *EPSL*, 38, 490–501, 2012.
- Nicholson, L., Prinz, R., Mölg, T., and Kaser, G.: Micrometeorological conditions and surface mass and energy fluxes on Lewis glacier, Mt Kenya, in relation to other tropical glaciers. *The Cryosphere*, 7, 1205–1225, doi:<http://dx.doi.org/10.5194/tc-7-1205-201310.5194/tc-7-1205-2013>, 2013.
- Østrem, G.: Ice melting under a thin layer of moraine, and the existence of ice cores in moraine ridges, *Geogr. Ann.*, 41, 228–230, 1959.
- Reid, T. D. and Brock, B. W.: An energy-balance model for debris-covered glaciers including heat conduction through the debris layer, *J. Glaciol.*, 56, 903–916, 2010.
- Reid, T. D., Carenzo, M., Pellicciotti, F., and Brock, B. W.: Including debris cover effects in a distributed model of glacier ablation, *J. Geophys. Res.*, 117, D18105, doi:<http://dx.doi.org/10.1029/2012JD01779510.1029/2012JD017795>, 2012.
- Reijmer, C. H. and Hock, R.: Internal accumulation on Storglacieren, Sweden, in a multi-layer snow model coupled to a distributed energy- and mass- balance model, *J. Glaciol.*, 54, 61–71, 2008.
- Reznichenko, N., Davies, T., Shulmeister, J., and McSaveney, M.: Effects of debris on ice-surface melting rates: an experimental

- study, *J. Glaciol.*, 56, 384–394, 2010.
- Sakai, A., Fujita, K., and Kubota, J.: Evaporation and percolation effect on melting at debris-covered Lirung Glacier, Nepal Himalayas, 1996, *Bull. Glaciol. Res.*, 21, 9–15, 2004.
- Sheng, D.: Review of fundamental principles in modelling unsaturated soil behaviour, *Comput. Geotech.*, 38, 757–776, 2011.
- Smith, G. D.: Numerical solution of partial differential equations: finite difference methods, 3rd edn., Oxford, Oxford University Press, 1985.
- Stokes, C. R., Popovnin, V., Aleynikov, A., Gurney, S. D., and Shahgedanova, M.: Recent glacier retreat in the Caucasus Mountains, Russia, and associated increase in supraglacial debris cover and supra-/proglacial lake development, *Ann. Glaciol.*, 46, 195–203, 2007.
- Webb, E. K., Pearman, G. I., and Leuning, R.: Correction of flux measurements for density effects due to heat and water vapour transfer, *Q. J. Roy. Meteor. Soc.*, 106, 85–100, 1980.
- Wilson, G. W., Fredlund, D. G., and Barbour, S.L.: Coupled soil-atmosphere modelling for soil evaporation, *Can. Geotech. J.*, 31, 151–161, 1994.
- Yeh, H-F., Lee, C.-C., and Lee, C.-H.: A rainfall-infiltration model for unsaturated soil slope stability, *J. Environ. Eng. Manage.* 18, 261–268, 2008.
- Zhang, Y., Fujita, K., Liu, S., Liu, Q., and Nuimura, T.: Distribution of debris thickness and its effect on ice melt at Hailuoguo glacier, southeastern Tibetan Plateau, using in situ surveys and ASTER imagery, *J. Glaciol.*, 57, 1147–1157, 2011.
- Zeng, Y., Su, Z., Wan, L., and Wen, J.: A simulation analysis of the advective effect on evaporation using a two-phase heat and mass flow model, *Water Res. Research*, 47, W10529, doi:<http://dx.doi.org/10.1029/2011WR010701>, 2011.

Table 1. Physical parameter values used in the CMB models. table

Density kg m^{-3}		
ice	915	–
whole rock	1496	Brock et al. (2010)
water	1000	–
Specific heat capacity $\text{J kg}^{-1} \text{K}^{-1}$		
air	1005	–
ice	2106	–
whole rock	948	Brock et al. (2010)
water	4181	–
Thermal conductivity $\text{W m}^{-1} \text{K}^{-1}$		
air	0.024	–
ice	2.51	–
whole rock	0.94	Reid and Brock (2010)
water	0.58	–
Surface roughness length [m^{-1}]		
ice	0.001	Reid and Brock (2010)
debris	0.016	Brock et al. (2010)
Albedo		
ice	0.34	Brock et al. (2010)
firn	0.52	Brock et al. (2010)
fresh snow	0.85	Mölg et al. (2012)
debris	0.13	Brock et al. (2010)
Emissivity		
ice/snow	0.97	Brock et al. (2010)
debris	0.94	Brock et al. (2010)

Table 2. Subsurface layer distribution and debris thickness used in this study.

Layers
Every 0.01 m from 0–0.24 m, 0.3, 0.4, 0.5, 0.8, 1.0, 1.4, 2.0, 3.0, 5.0, 7.0, 9.0 m
Debris thickness
0.23 m

Table 3. Mean deviation (MD), mean absolute deviation (MAD), and R value for the evaluation variables of surface temperature (T_{sfc}), and the turbulent fluxes of sensible (QS) and latent heat (QL).

2008		CMB-DRY	CMB-RES
T_{sfc}	MD	-0.5	-1.1
	MAD	2.3	2.4
	R	0.94	0.94
QS	MD	-65.2	-47.0
	MAD	71.1	54.2
	R	0.91	0.92
QL	MD	23.9	1.0
	MAD	28.2	19.1
	R	-	0.52
2011		CMB-DRY	CMB-RES
T_{sfc}	MD	1.1	0.9
	MAD	1.9	1.7
	R	0.97	0.97

Table 4. Average-energy and accumulated-mass fluxes at the surface over the 2008 simulation for CMB-RES and CMB-DRY.

average W m^{-2}	CMB-DRY	CMB-RES
net shortwave (SWnet)	237.6	237.6
net longwave (LWnet)	-91.0	-87.8
conduction (QC)	-41.5	-40.1
sensible heat (QS)	-104.2	-86.0
latent heat (QL)	-	-22.9
precipitation (QPRC)	-0.9	-0.7
sum kg m^{-2}	CMB-DRY	CMB-RES
melt	-	0.
refreeze	-	0.
sublimation	-	0.
deposition	-	0.
evaporation	-	17.3
condensation	-	0.1
sub-debris ice melt	241.3	233.8

Table 5. Average-energy and accumulated-mass fluxes at the surface over the 2011 simulation for CMB-RES and CMB-DRY.

average W m^{-2}	CMB-DRY	CMB-RES
net shortwave (SWnet)	133.0	133.0
net longwave (LWnet)	-80.2	-78.8
conduction (QC)	-23.0	-22.4
sensible heat (QS)	-27.0	-20.0
latent heat (QL)	-	-9.8
precipitation (QPRC)	-0.1	-0.1
sum kg m^{-2}	CMB-DRY	CMB-RES
melt	4.6	4.4
refreeze	0	0
sublimation	0.2	0.5
deposition	0	0
evaporation	-	8.6
condensation	-	0.1
sub-debris ice melt	172.4	160.4

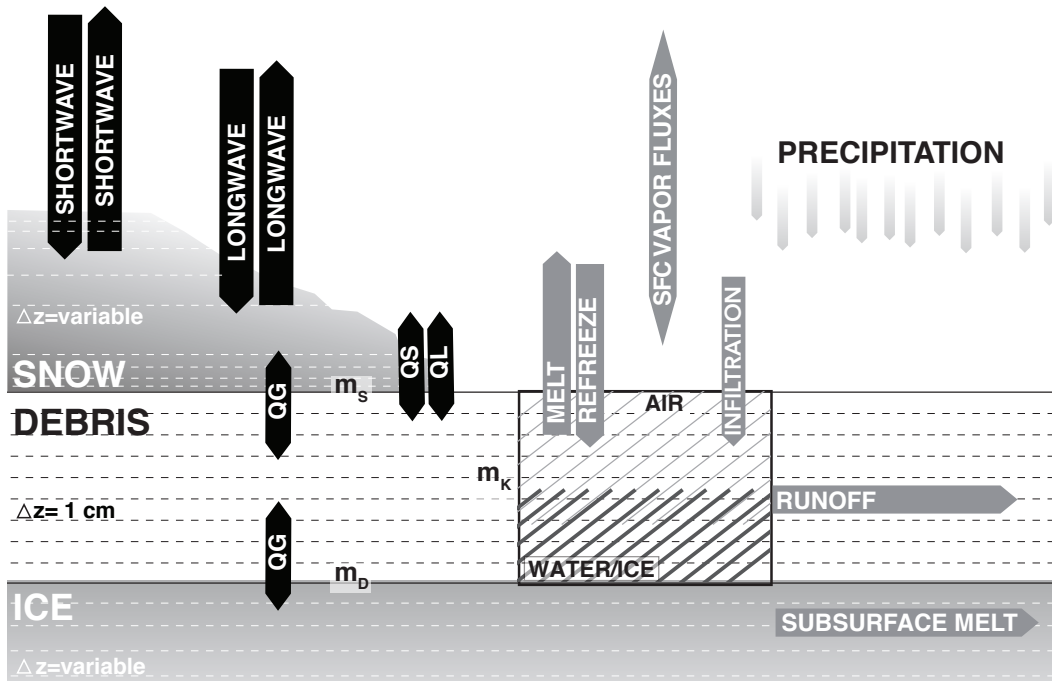


Fig. 1. Schematic of the CMB-RES model and its treatment of the debris moisture content and its phase. The levels m_s , m_D , and m_K correspond to the bottom of the snowpack, the base of the debris layer, and the level of the saturated horizon, respectively.

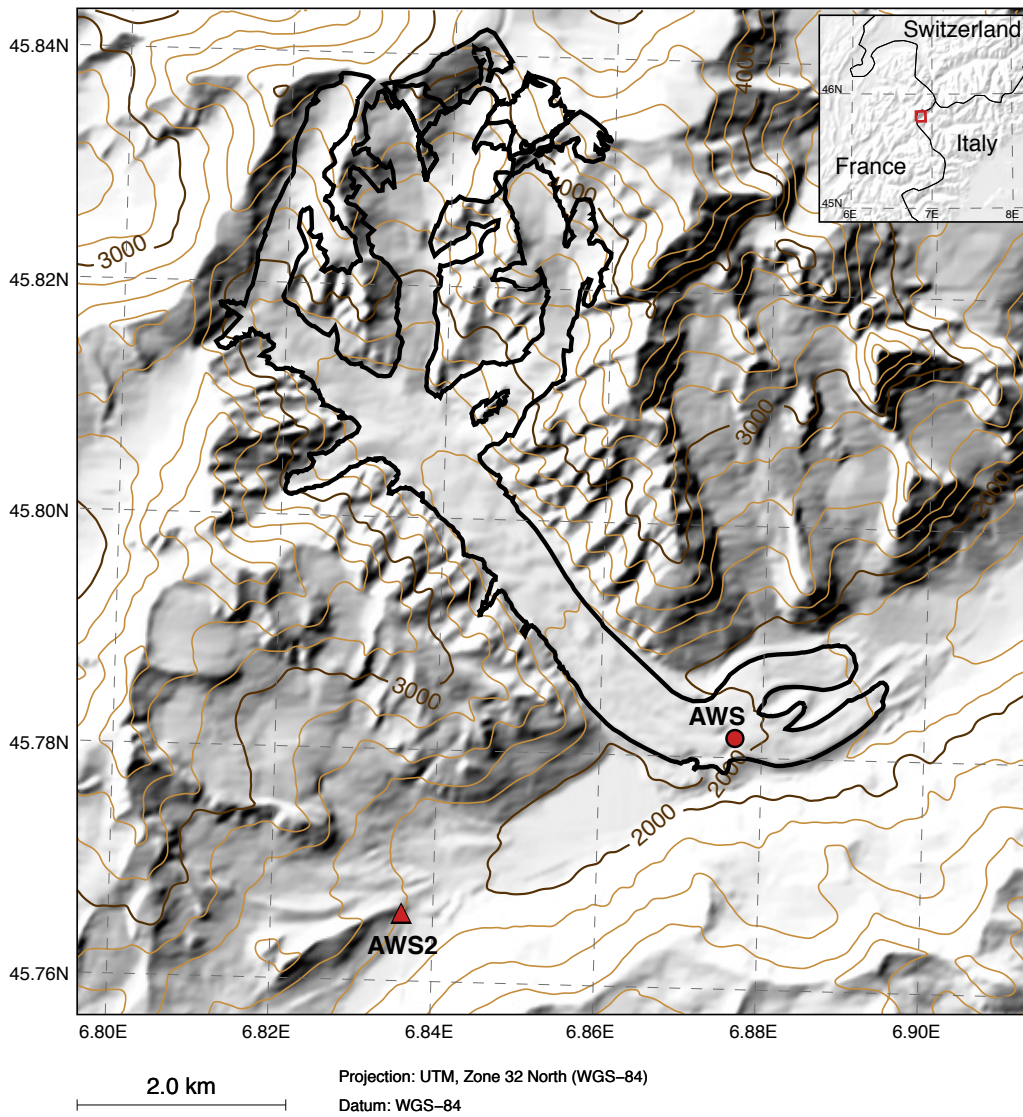


Fig. 2. Map showing the location of Miage glacier. The AWS located on the glacier is denoted with a red circle and the AWS2 from which precipitation data were obtained is shown by a red triangle.

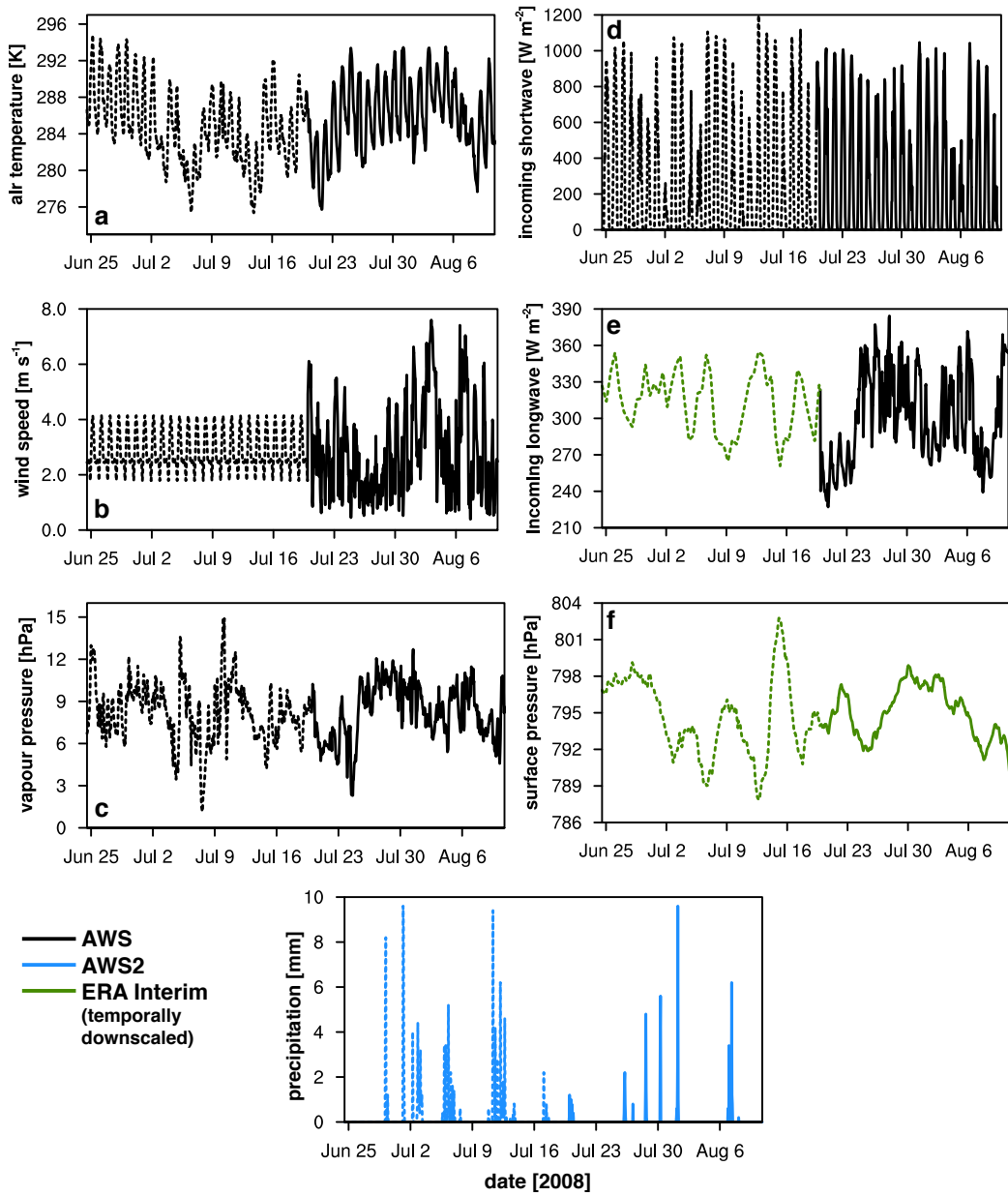


Fig. 3. Times series from the 2008 simulation of the forcing variables of (a) 2 m air temperature [K], (b) wind speed [m s^{-1}], (c) 2 m vapour pressure [hPa], (d) incoming shortwave radiation [W m^{-2}], (e) incoming longwave radiation [W m^{-2}], (f) surface pressure [hPa], and (g) precipitation [mm]. Data from the AWS on the Miage glacier are shown in black, from the second AWS (4 km away) in blue, and temporally downscaled from the ERA-Interim reanalysis in green. Dashed curves indicate the discarded spin-up period, while solid curves indicate the simulation time.

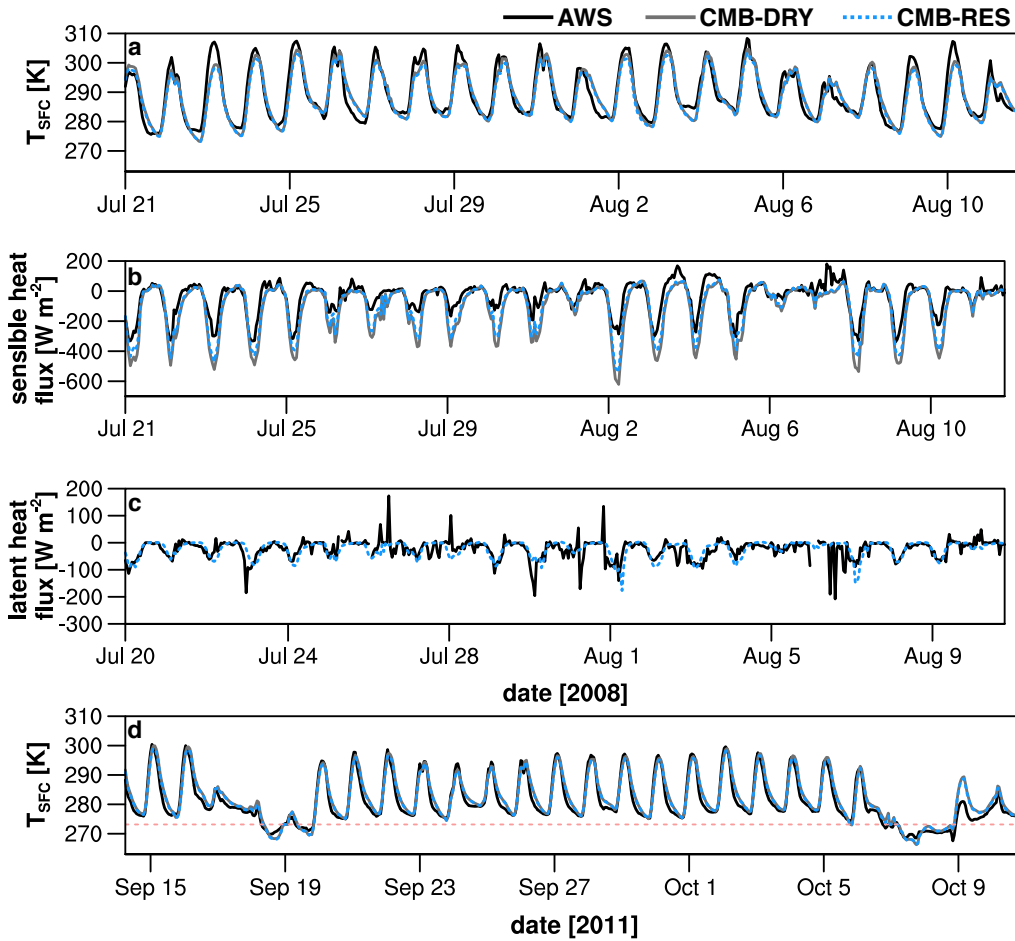


Fig. 4. Time series from the 2008 simulation of (a) debris surface temperature (T_{sfc} ; [K]) and the turbulent fluxes of (b) sensible and (c) latent heat [W m^{-2}], for measurements (black curve), CMB-DRY (dark grey curve), and CMB-RES (blue, dashed curve). (d) Same as panel a, but for the 2011 simulation. The horizontal dashed red line indicates the freezing point, 273.15 K.

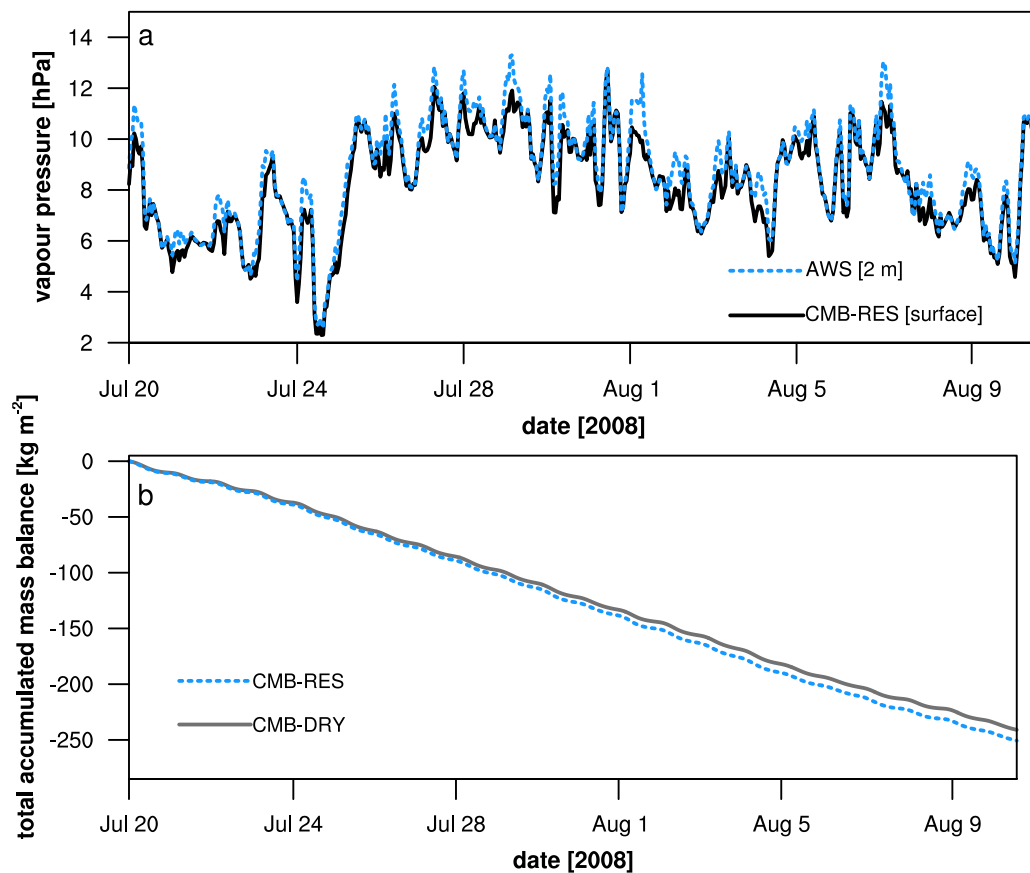


Fig. 5. Time series from the 2008 simulation of (a) surface (dashed-blue curve) and 2 m air (black curve) vapour pressure [hPa] in CMB-RES, and (b) total accumulated mass balance [kg m^{-2}] for CMB-DRY (solid-grey curve) and CMB-RES (dashed-blue curve).

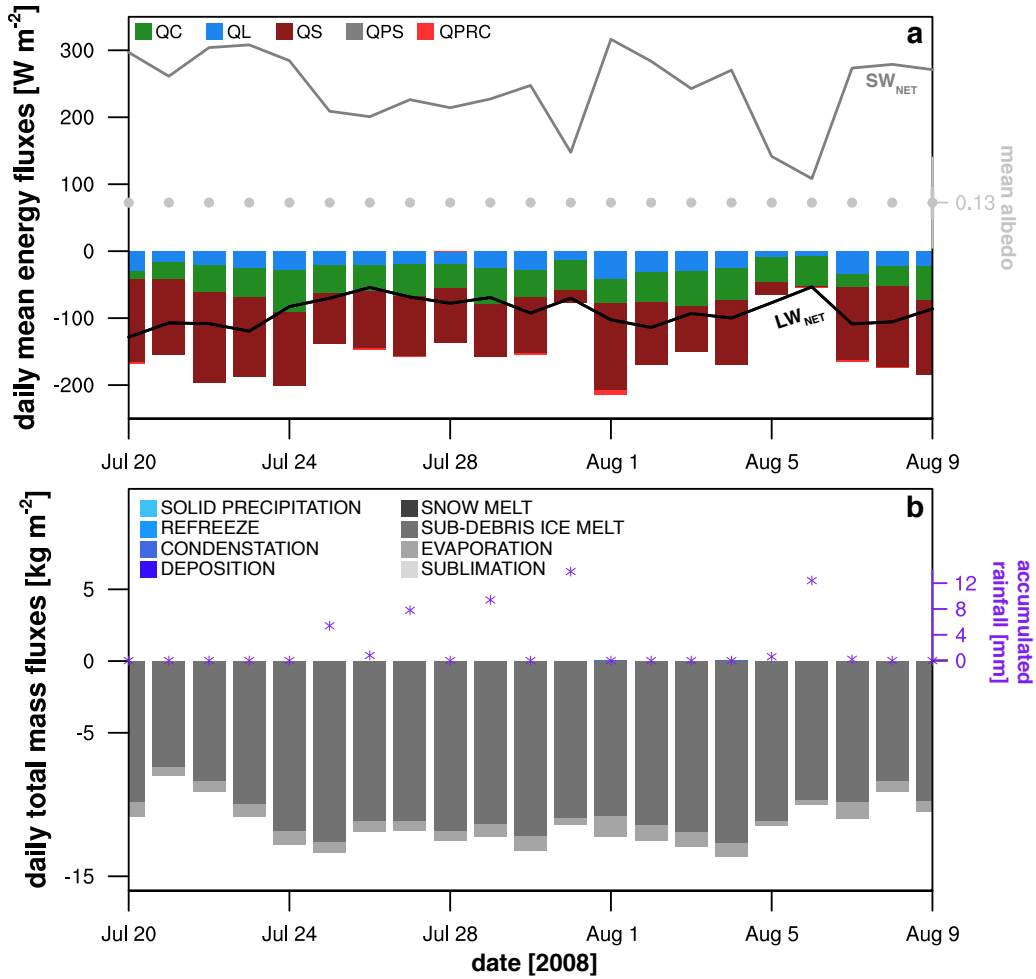


Fig. 6. CMB-RES values for (a) daily mean energy fluxes over the evaluation period [W m^{-2}]. The grey curve is net shortwave radiation, the black curve is net longwave radiation, and the grey dots show daily-mean surface albedo, which remains constant at the debris value because there is no solid precipitation. (b) Daily total mass fluxes [kg m^{-2}]. Maximum daily values of evaporation and condensation are 1.4 and 0.02 kg m^{-2} , respectively, although the latter flux is not visible. Note that while daily-accumulated rainfall is shown (purple asterisks), it is not technically a mass flux, since the mass balance calculation in CMB-RES does not account for debris water storage. Rather, this field is plotted to show its correspondence with other fields, such as net shortwave radiation.

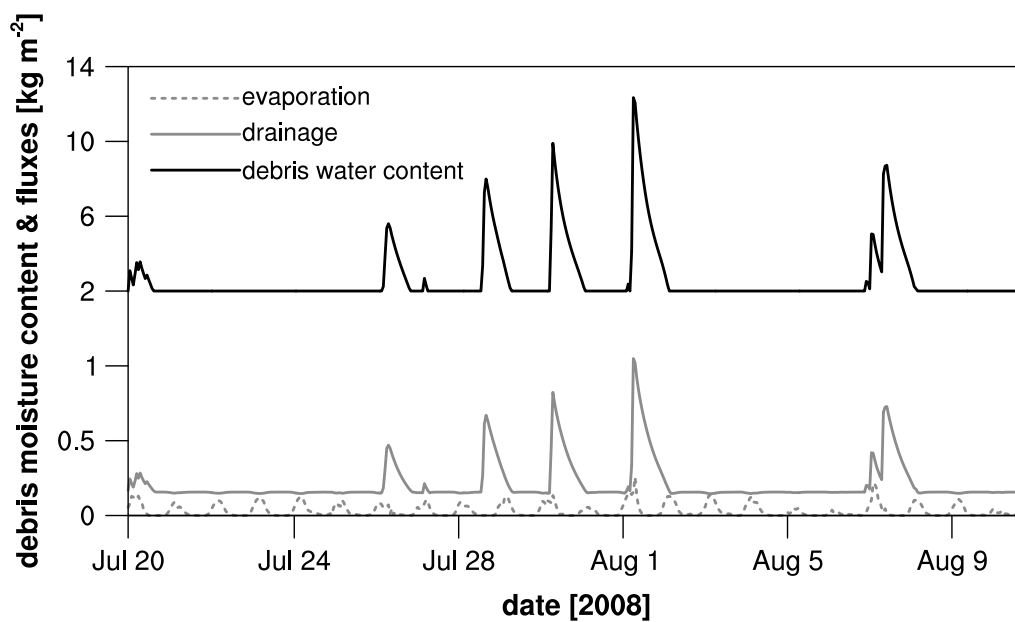


Fig. 7. Time series of total debris water content (black curve) as well as the two sources of debris water loss: horizontal drainage (solid-grey curve) and evaporation (dashed- grey curve). Units are kg m^{-2} .

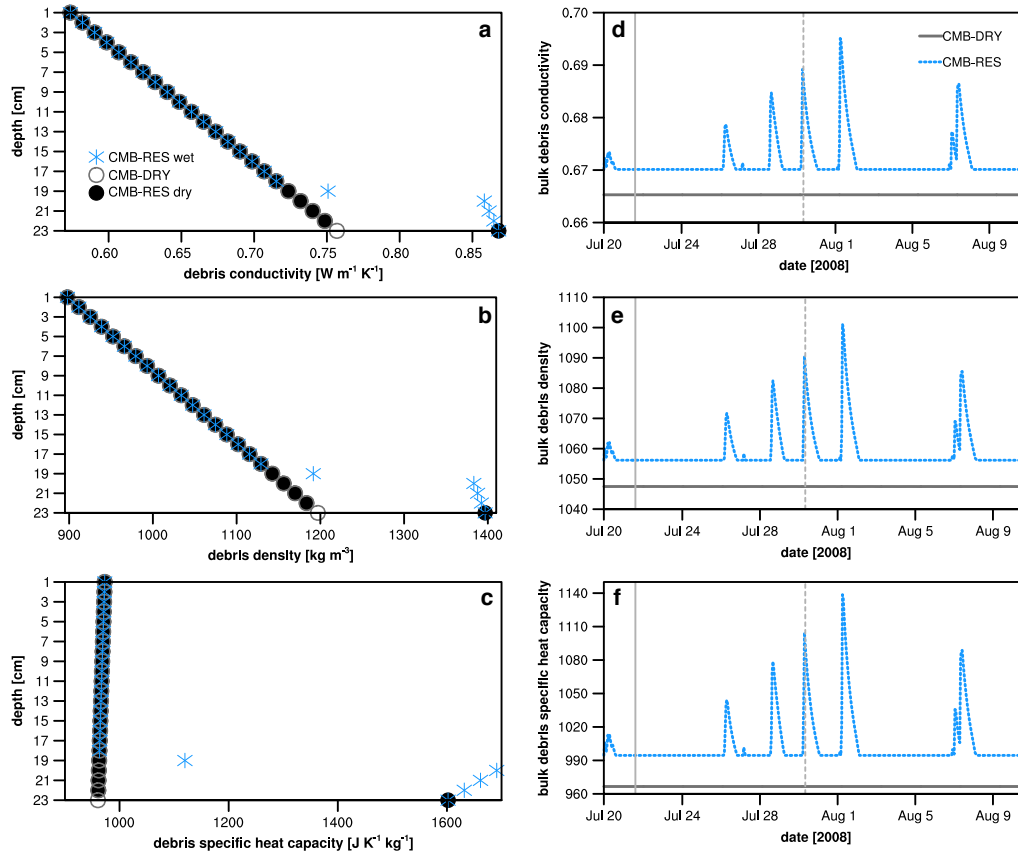


Fig. 8. Depth variation of (a) debris thermal conductivity [$\text{W m}^{-1} \text{K}^{-1}$], (b) density [kg m^{-3}], and (c) specific heat capacity [$\text{J kg}^{-1} \text{K}^{-1}$], shown for CMB-DRY in grey-unfilled circles and for CMB-RES in both black-filled circles (“dry” time slice) and blue asterisks (“wet” time slice). Time series of bulk values for these same properties are shown in panels (d–f) for CMB-RES in blue and CMB-DRY in grey. The locations of the “dry” and “wet” time slices are indicated by the first (solid grey) and second (dashed grey) reference lines on the x-axis, respectively.

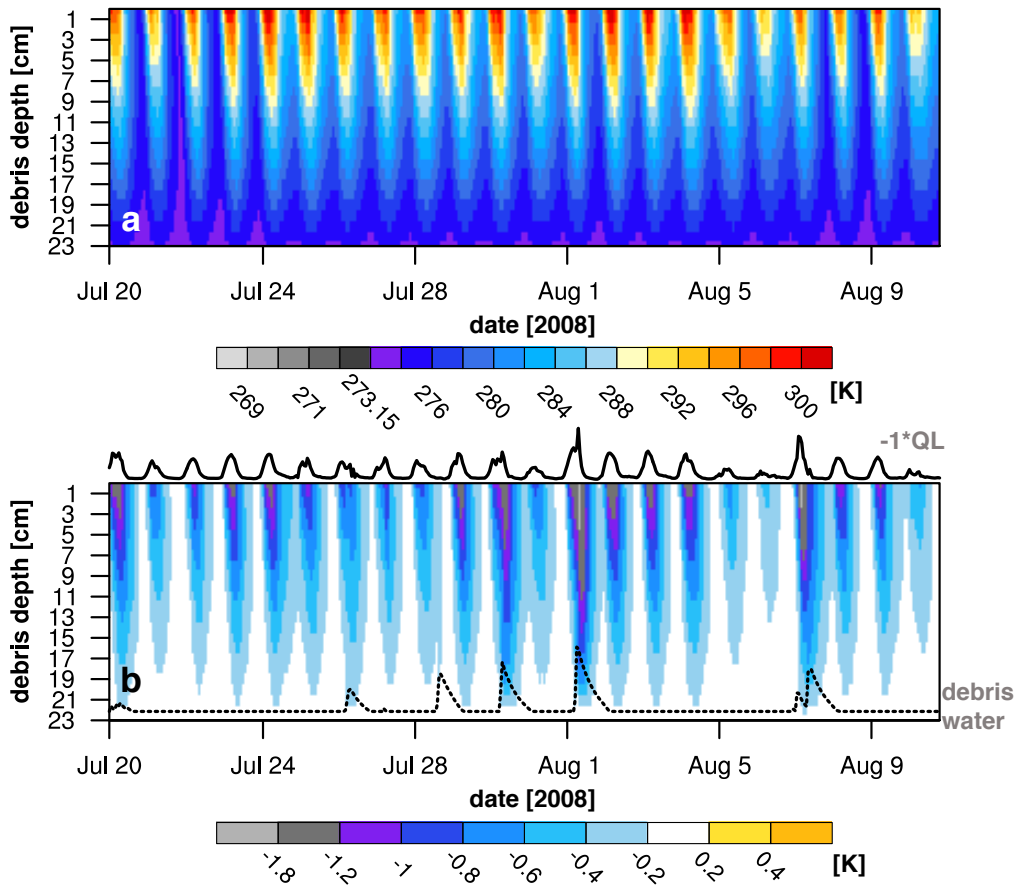


Fig. 9. Temporal and depth variation of (a) CMB-RES debris temperature and (b) the difference between the model runs (CMB-RES minus CMB-DRY). Units are K. For reference, $-1 \cdot QL$ (solid-black curve; now positive for energy loss from the surface) and debris water content (black dashed) are plotted without y-axes in panel (b). The height of the debris-water curve shows the estimated level of moisture in the reservoir.

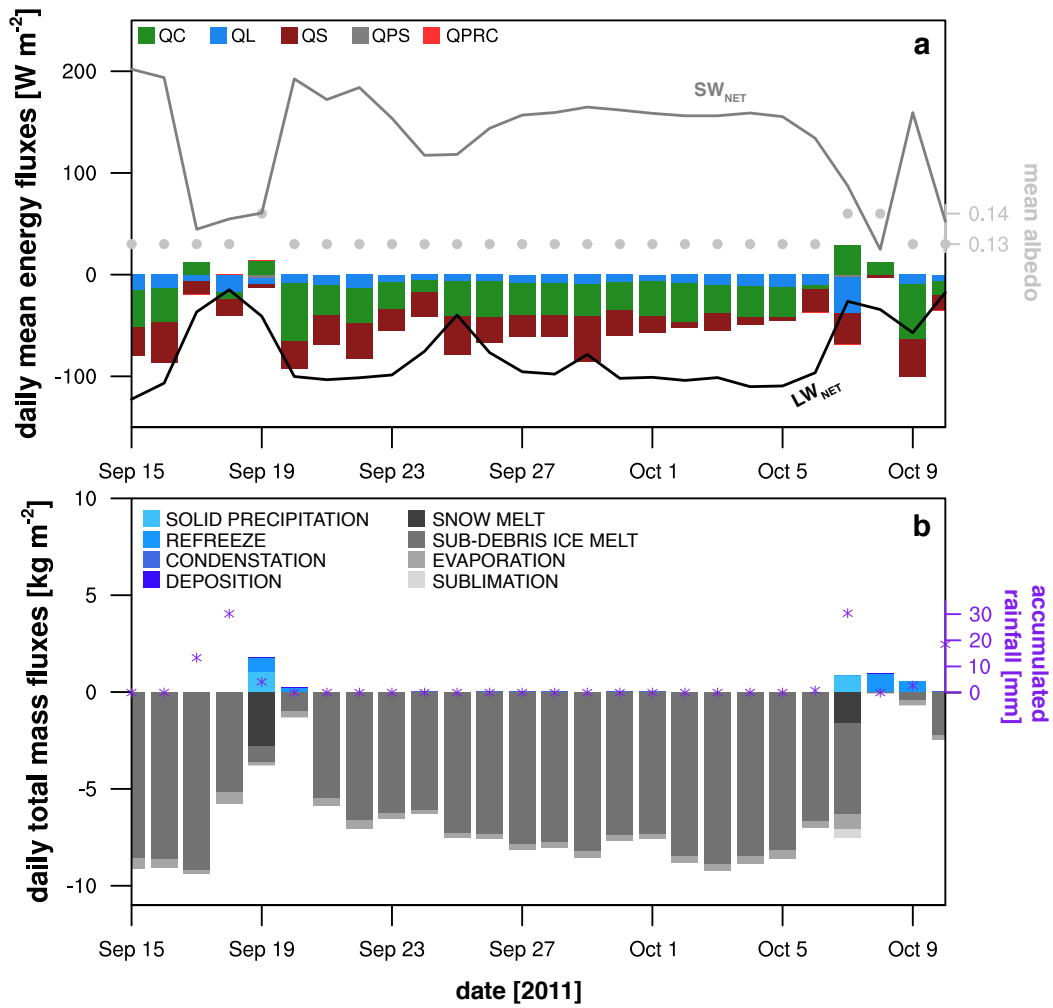


Fig. 10. Same as Fig. 6 but for the 2011 simulation.

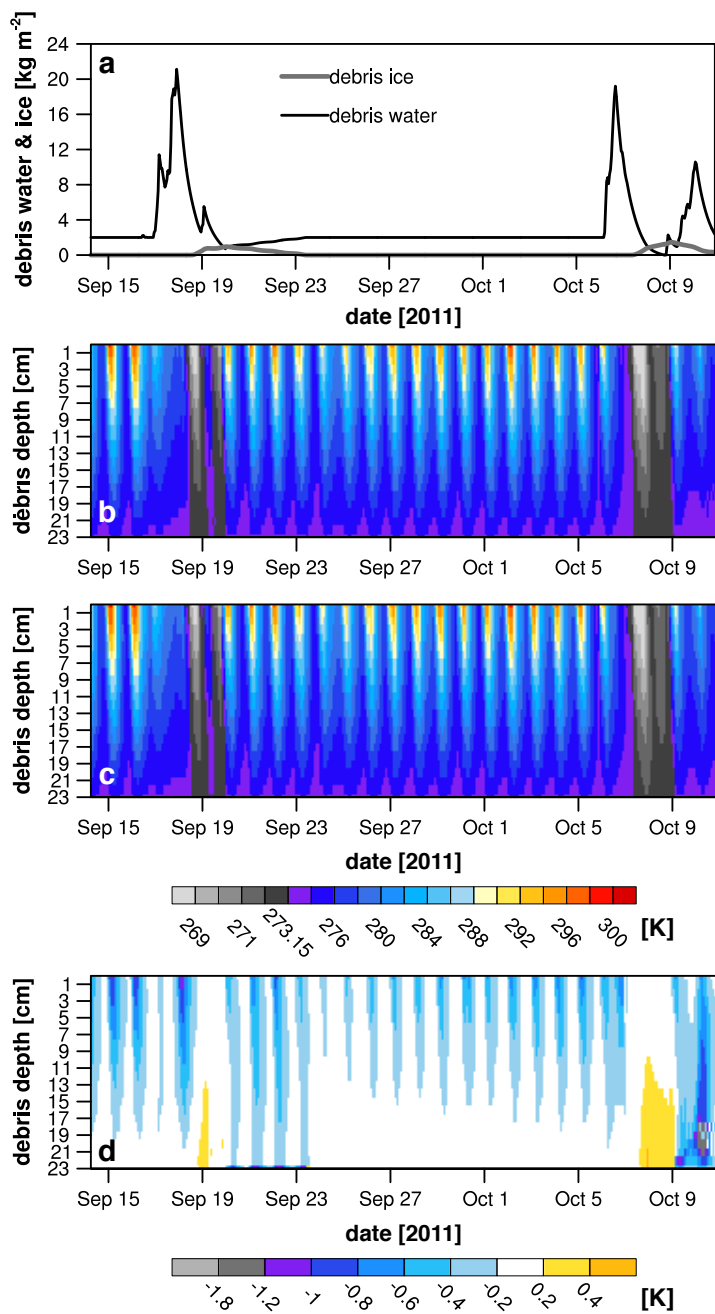


Fig. 11. (a) Time series from the 2011 simulation of the debris water (black line) and ice (grey line) content kg m^{-2} . Temporal and depth variation of the debris temperatures in (b) CMB-RES and (c) CMB-DRY, and (d) the difference between the model runs (CMB-RES minus CMB-DRY). Units are K.

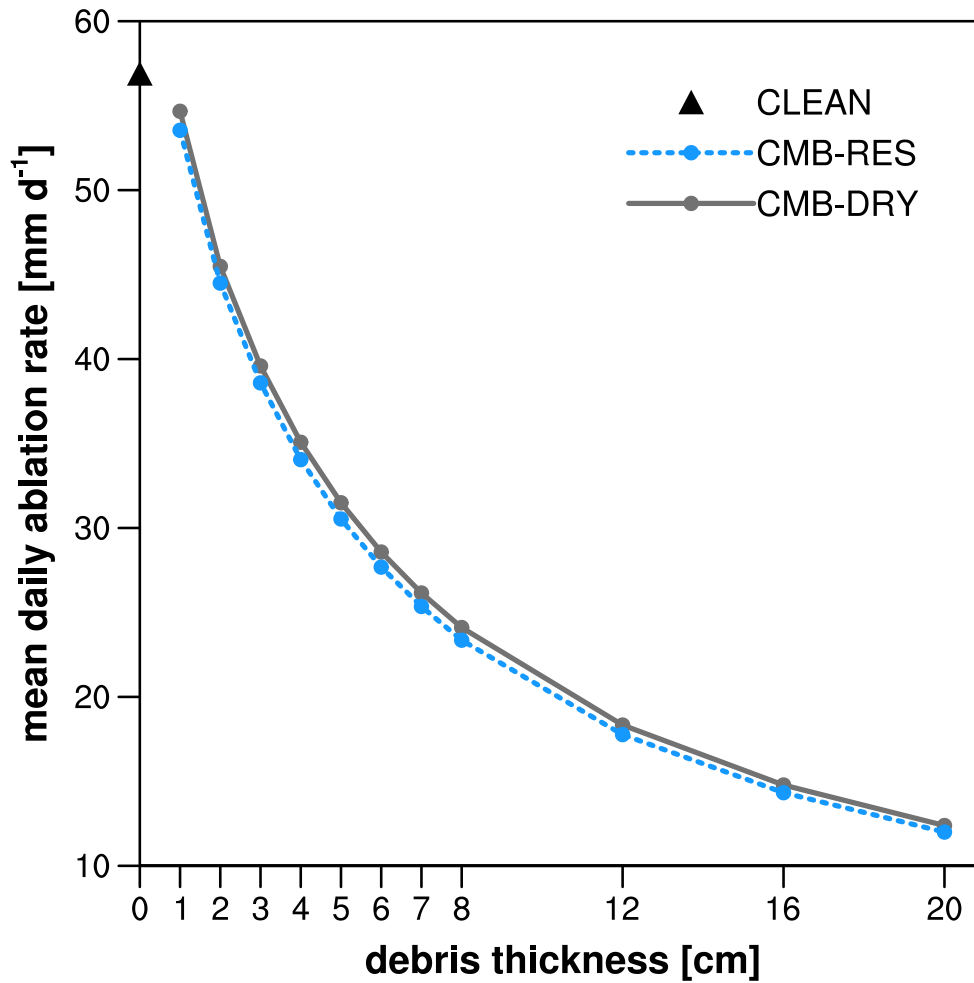


Fig. 12. Daily mean sub-debris ice ablation rate [mm w.e. d⁻¹] vs. debris thickness [cm], produced by the CMB models using the forcing data from the 2008 simulation. The clean ice melt rate is represented by a black triangle. CMB-DRY is the solid-grey curve and CMB-RES is the dashed-blue curve.